Azide-bridged Cu(II), Mn(II) and Co(II) coordination polymers constructed with a bifunctional ligand of 6-(1H-tetrazol-5-yl)-2,2'-bipyridine

Jung-Yu Tsao, Jia-Dong Tsai and Chen-I Yang*

Department of Chemistry, Tunghai University, Taichung 407, Taiwan

Table S1. Selected bond distances (Å) and angles (°) for compounds **1·Cu**, **2·Mn** and **3·Co**.

1·Cu			
Cu(1)-N(2)	1.828(2)	Cu(1)-N(1)	1.986(2)
Cu(1)-N(3)	1.886(3)	Cu(1)-N(7)	2.048(3)
N(2)-Cu(1)-N(3)	87.21(12)	N(2)-Cu(1)-N(7)	156.26(11)
N(2)-Cu(1)-N(1)	73.65(10)	N(3)-Cu(1)-N(7)	98.87(11)
N(3)-Cu(1)-N(1)	160.65(11)	N(1)-Cu(1)-N(7)	97.66(10)

2·Mn			
Mn(1)-N(7)	2.195(2)	Mn(1)-N(6)	2.2857(19)
Mn(1)-N(7)#1	2.219(2)	Mn(1)-N(3)	2.286(2)
Mn(1)-N(2)	2.2452(19)	Mn(1)-N(1)	2.318(2)
N(7)-Mn(1)-N(7)#1	76.73(8)	N(7)#1-Mn(1)-N(3)	124.58(8)
N(7)-Mn(1)-N(2)	112.10(7)	N(2)-Mn(1)-N(3)	71.79(7)
N(7)#1-Mn(1)-N(2)	162.28(8)	N(6)-Mn(1)-N(3)	91.00(7)
N(7)-Mn(1)-N(6)	160.71(8)	N(7)-Mn(1)-N(1)	93.43(7)
N(7)#1-Mn(1)-N(6)	86.23(7)	N(7)#1-Mn(1)-N(1)	94.16(8)
N(2)-Mn(1)-N(6)	86.78(7)	N(2)-Mn(1)-N(1)	70.54(7)
N(7)-Mn(1)-N(3)	91.31(7)	N(6)-Mn(1)-N(1)	96.78(7)
N(3)-Mn(1)-N(1)	140.96(7)	Mn(1)-N(7)-Mn(1)#1	103.27(8)

Symmetry transformations used to generate equivalent atoms:
#1 -x+2,-y,-z+1

3·Co			
Co(1)-N(7)	2.0276(12)	Co(1)-N(3)	2.1548(12)
Co(1)-N(2)	2.0861(12)	Co(1)-N(1)	2.1569(12)
Co(1)-N(5)#1	2.1483(12)	Co(1)-N(7)#2	2.2966(12)
N(7)-Co(1)-N(2)	160.68(5)	N(5)#1-Co(1)-N(1)	89.12(5)
N(7)-Co(1)-N(5)#1	100.75(5)	N(3)-Co(1)-N(1)	151.76(5)
N(2)-Co(1)-N(5)#1	97.01(5)	N(7)-Co(1)-N(7)#2	78.11(5)
N(7)-Co(1)-N(3)	110.19(5)	N(2)-Co(1)-N(7)#2	83.92(4)
N(2)-Co(1)-N(3)	76.45(5)	N(5)#1-Co(1)-N(7)#2	178.08(4)
N(5)#1-Co(1)-N(3)	92.18(5)	N(3)-Co(1)-N(7)#2	89.68(4)
N(7)-Co(1)-N(1)	97.23(5)	N(1)-Co(1)-N(7)#2	89.49(5)
Co(1)-N(7)-Co(1)#2	101.89(5)		

Symmetry transformations used to generate equivalent atoms:
#1 x,-y+5/2,z+1/2 #2 -x+1,-y+2,-z+1

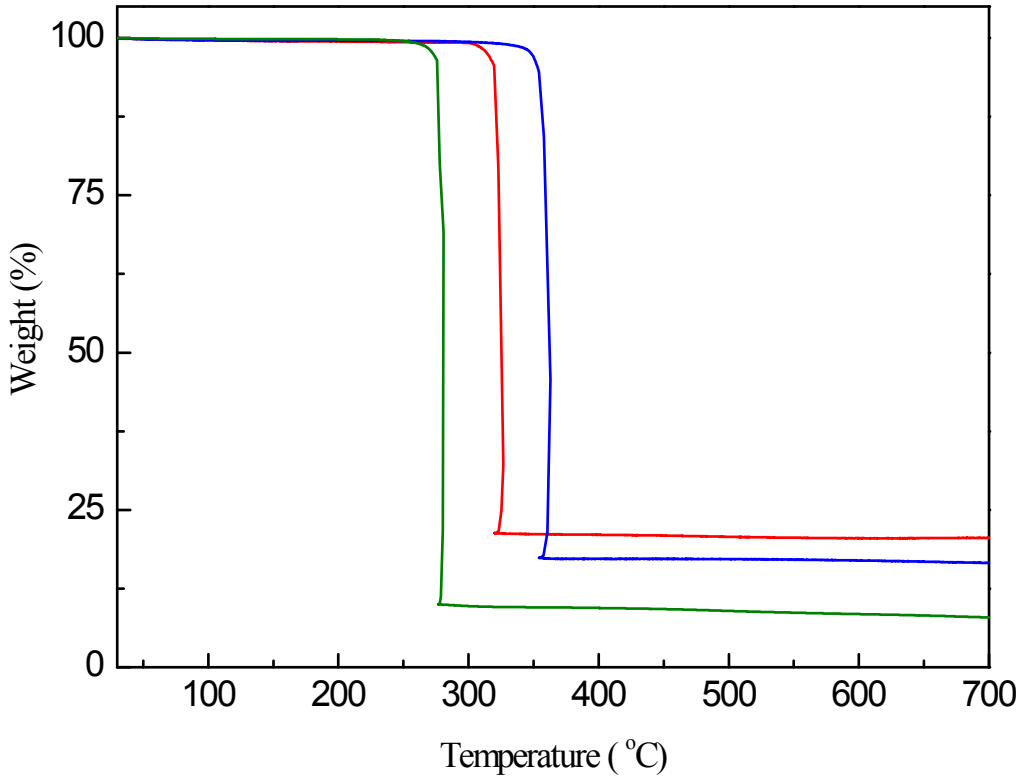

Fig. S1. Thermogravimetric (TG) analysis diagrams of **1·Cu** (green line), **2·Mn** (blue line), and **3·Co** (red line).

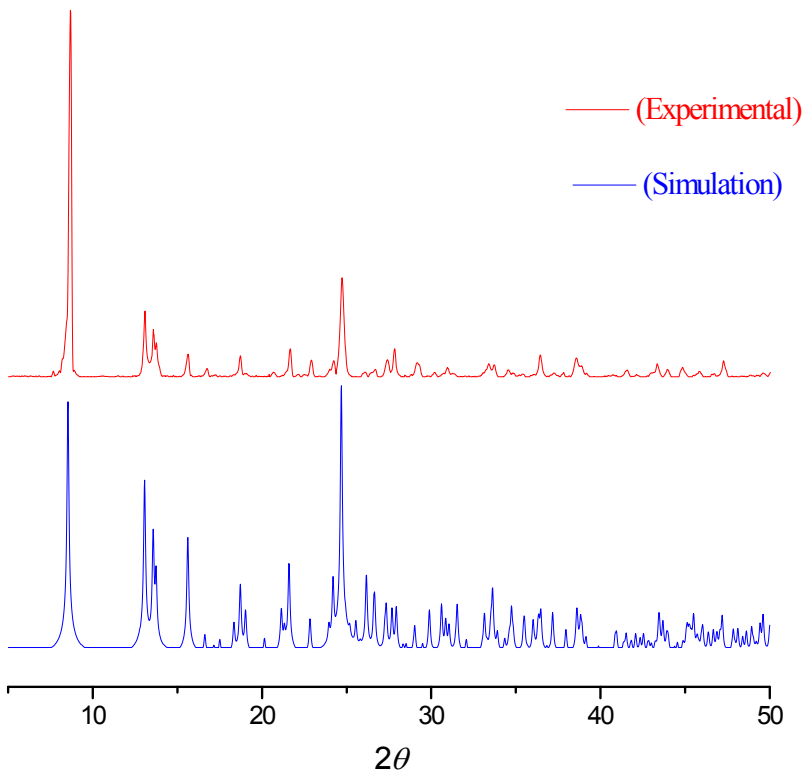

Fig. S2. Simulated PXRD pattern (red) and experimental PXRD pattern of compound **1·Cu.**

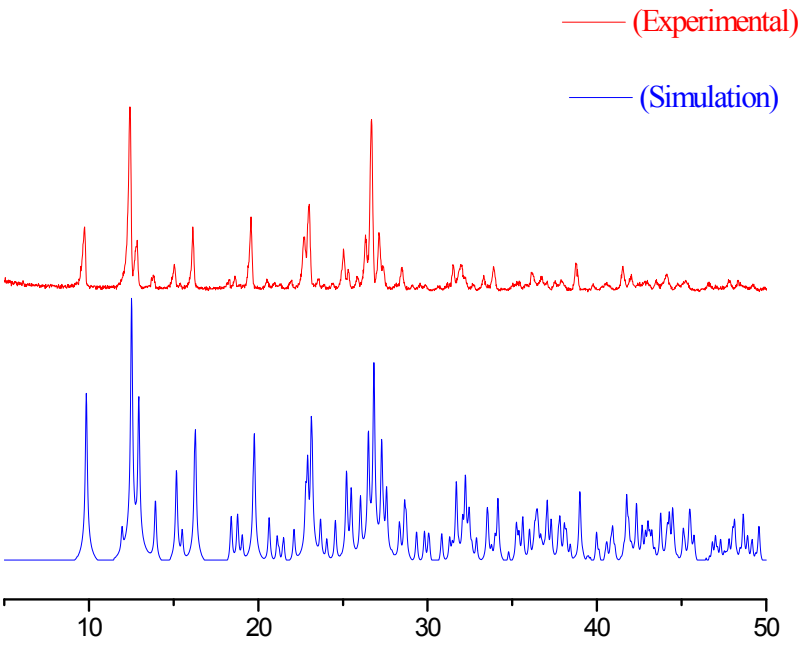

Fig. S3. Simulated PXRD pattern (red) and experimental PXRD pattern of compound **2·Mn.**

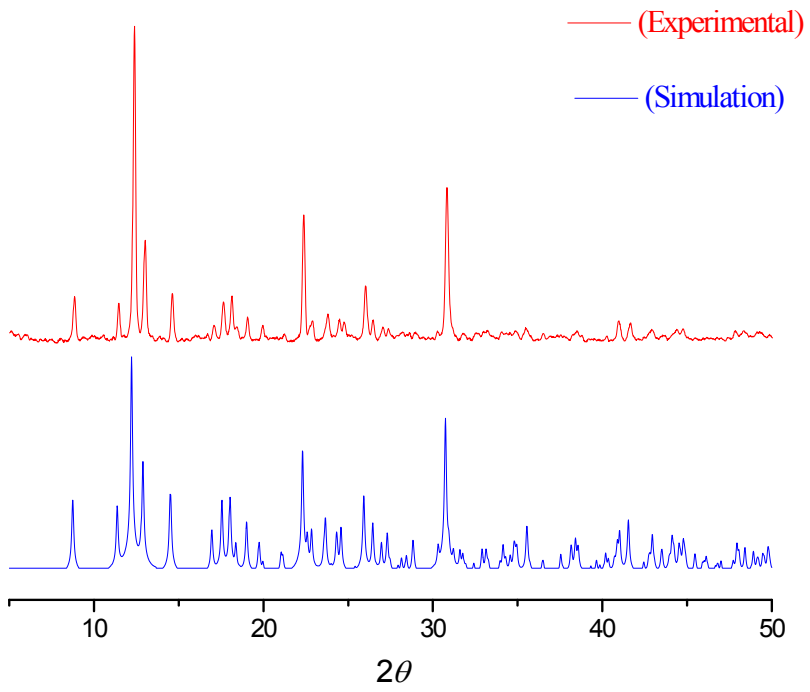

Fig. S4. Simulated PXRD pattern (red) and experimental PXRD pattern of compound **3·Co.**

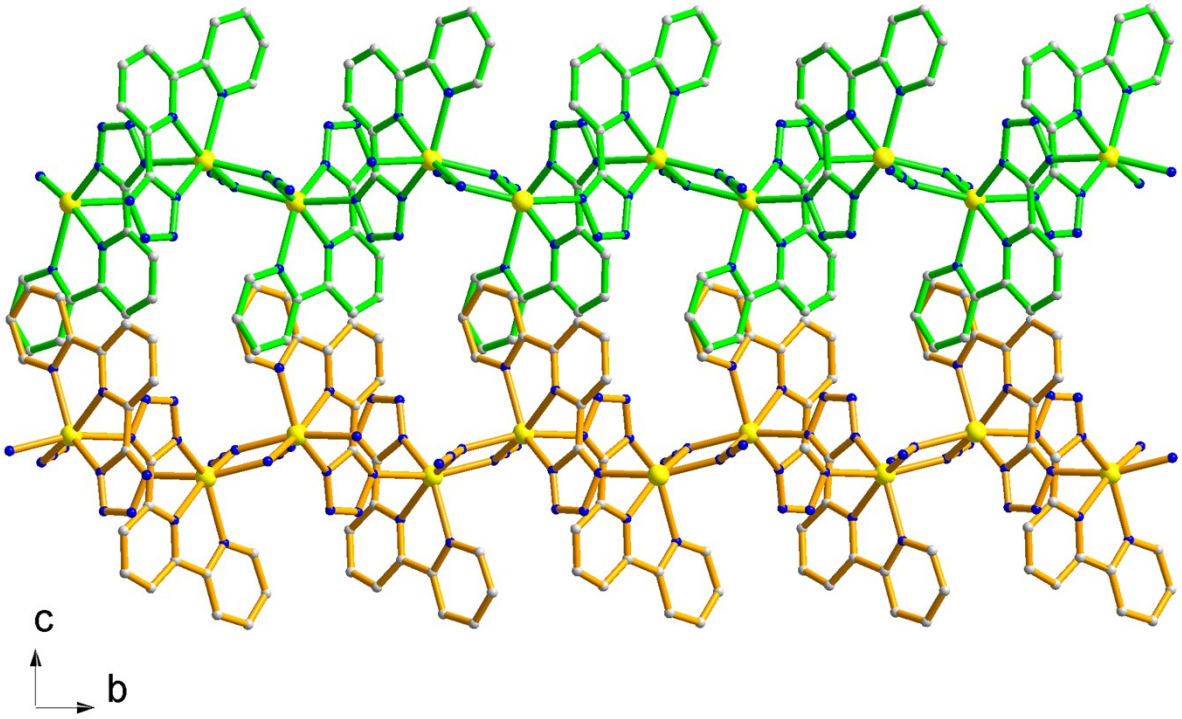

Fig. S5. Perspective view of interlayer π-π interactions in **2·Mn**.

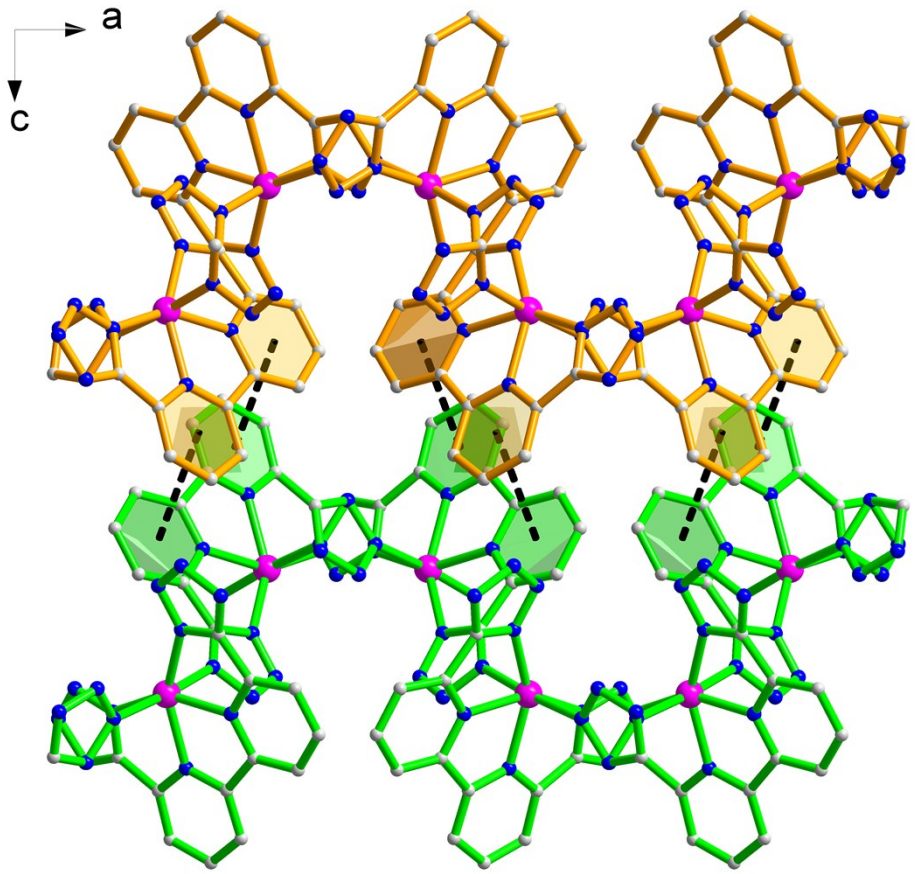

Fig. S6. Perspective view of interlayer π-π interactions in **3·Co**.

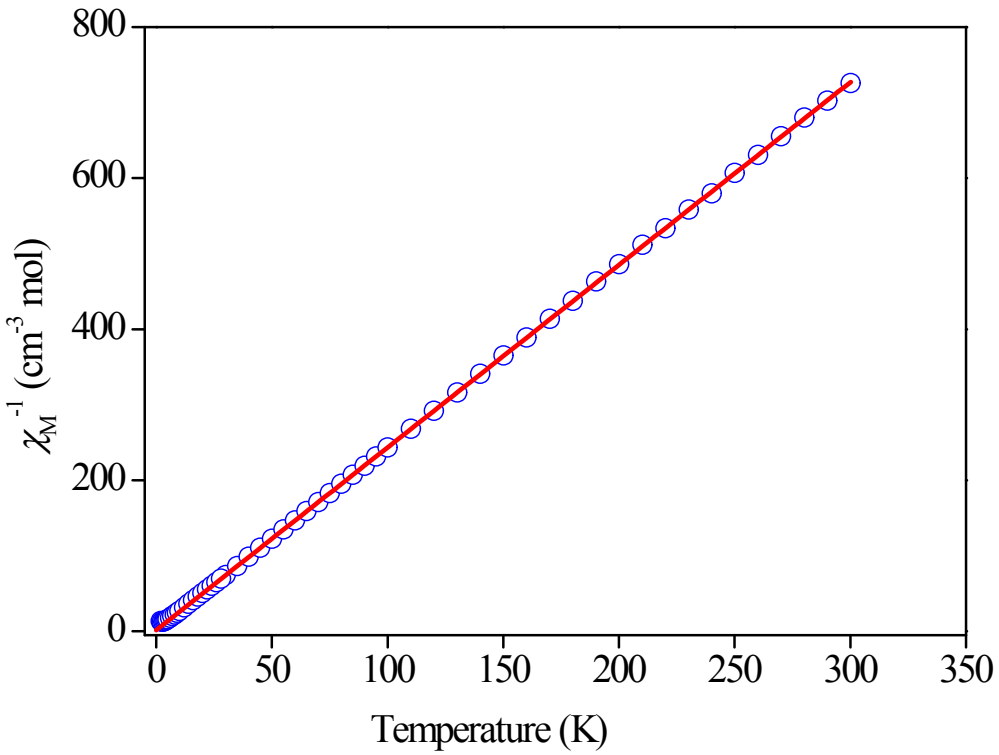

Fig. S7. Plot of χ_M^{-1} (○) vs. *T* of compound **1·Cu**. The solid line represents the best fit χ_M^{-1} above 30 K with a Curie–Weiss law.

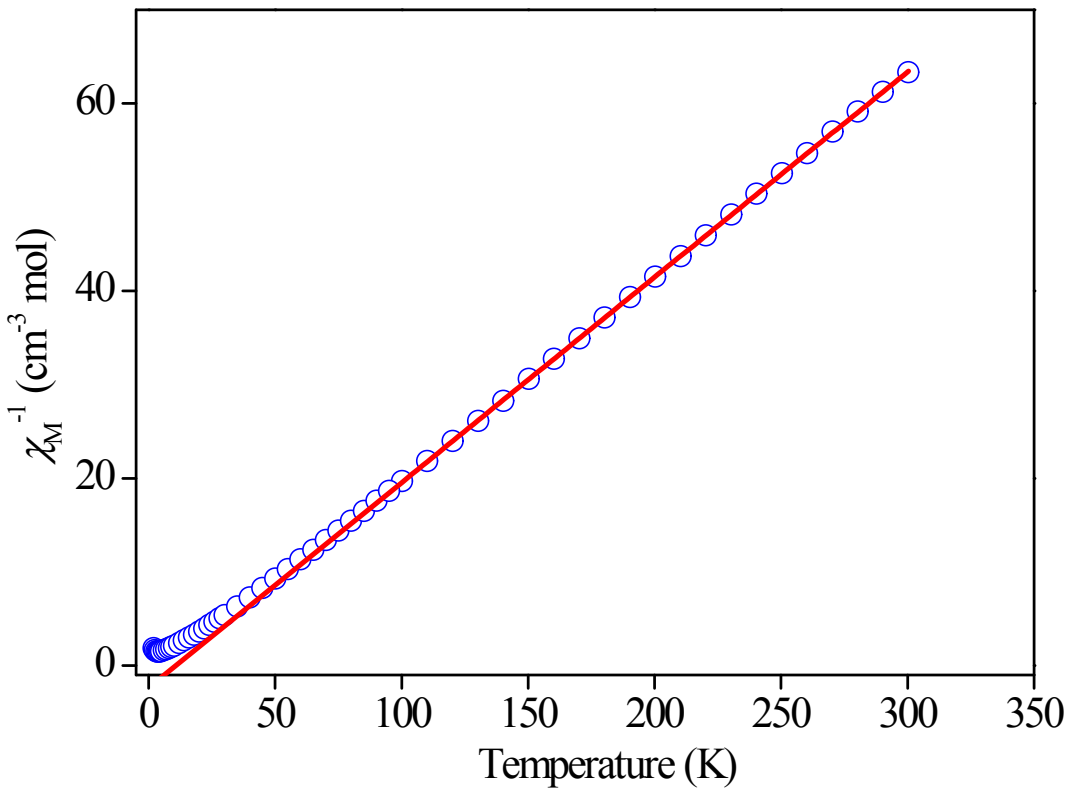

Fig. S8. Plot of χ_M^{-1} (○) vs. *T* of compound **2·Mn**. The solid line represents the best fit χ_M^{-1} above 100 K with a Curie–Weiss law.

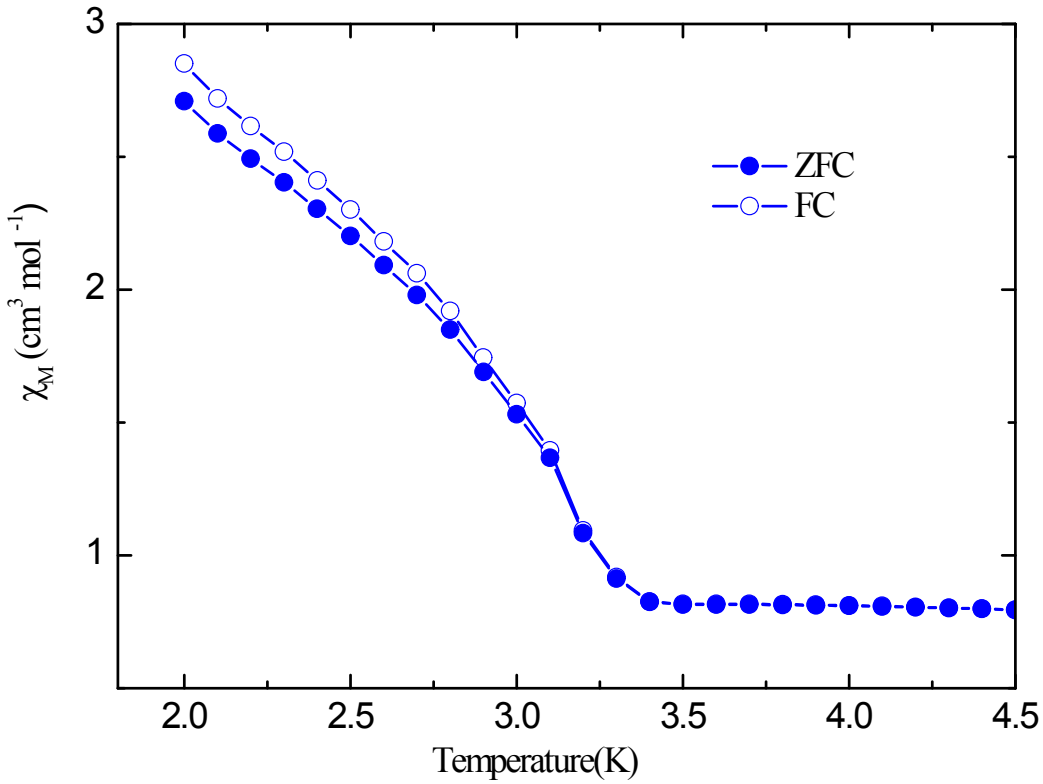

Fig. S9. ZFC/FC magnetizations of compound **2·Mn** at the field of 20 Oe.

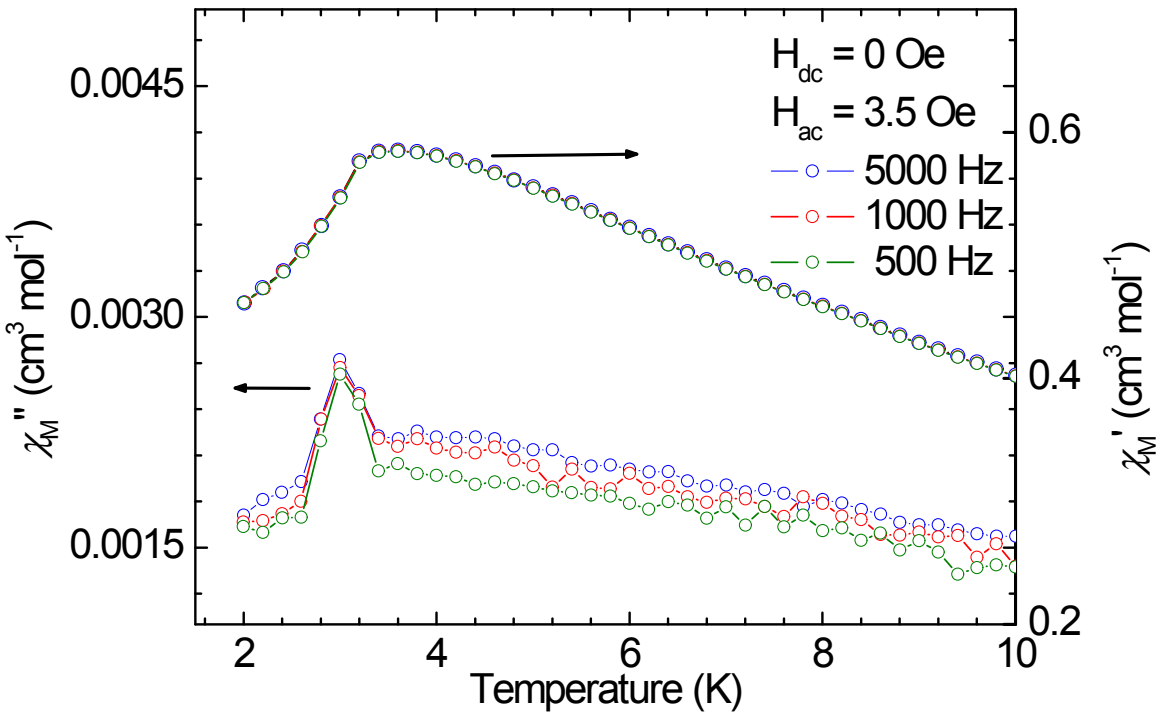

Fig. S10. In phase (χ′) and out-off phase (χ″) of the ac magnetic susceptibilities in a zero applied dc field and a 3.5 G ac field at the indicated frequencies for compound **2·Mn**.

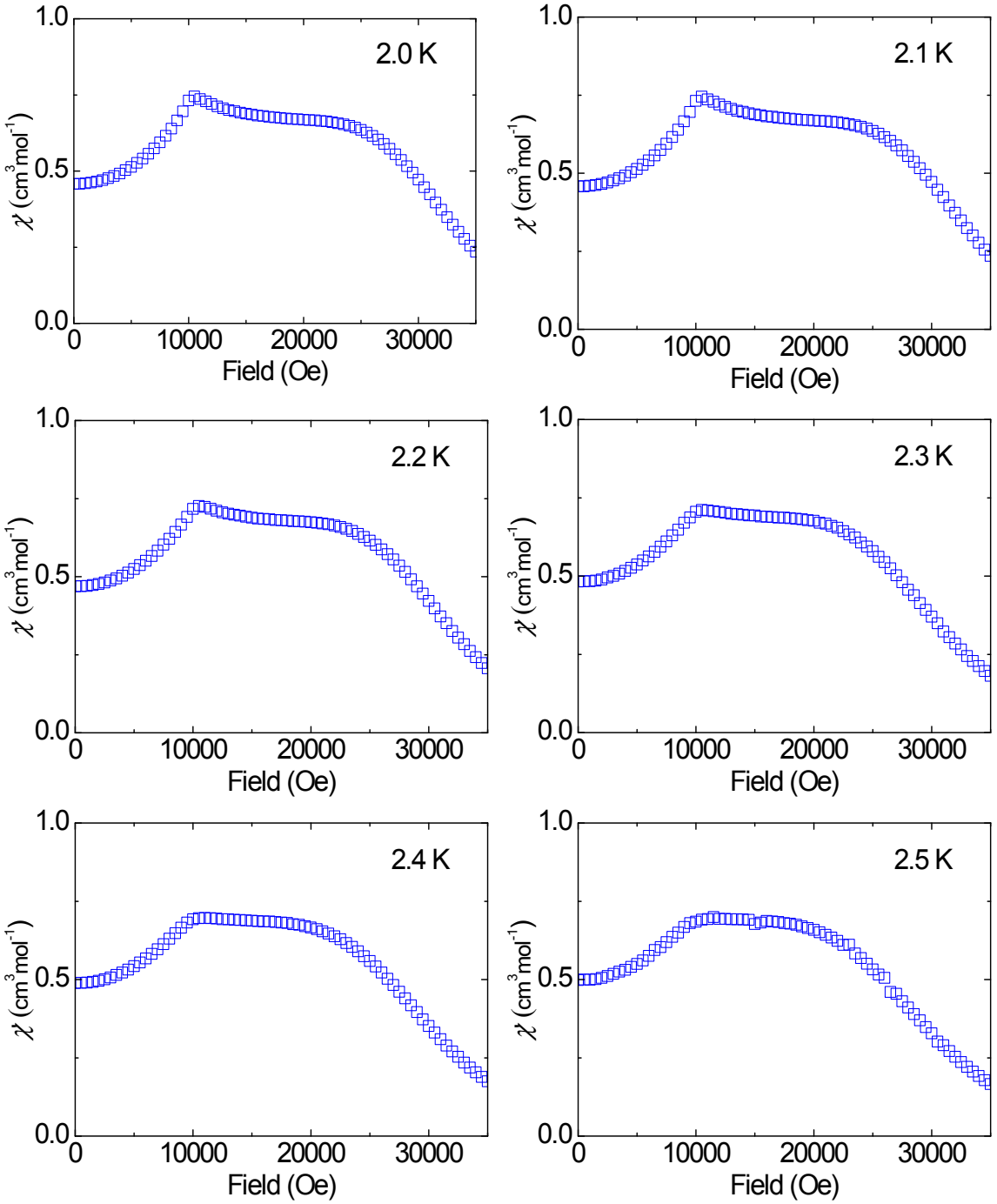

Fig. S11. χ_M' vs. H plots for field dependence of the ac magnetic susceptibilities in a zero applied dc field and in an 3.5 Oe ac field and 100 Hz at the indicated temperatures for **2·Mn**.

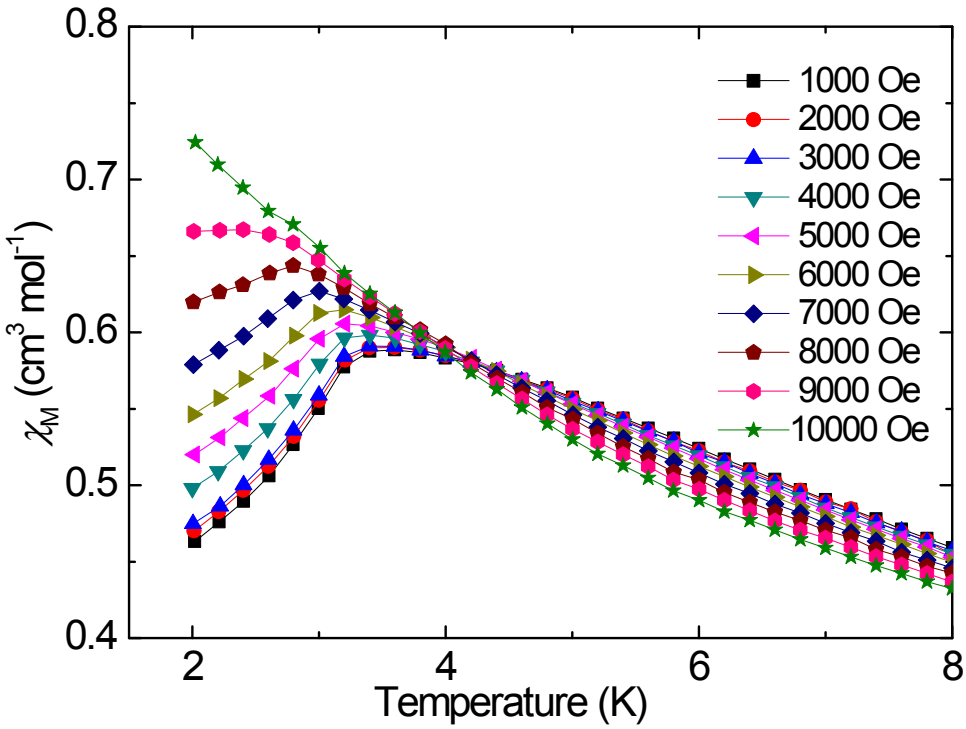

Fig. S12. FC magnetizations of compound **2·Mn** under the indicated applied fields.

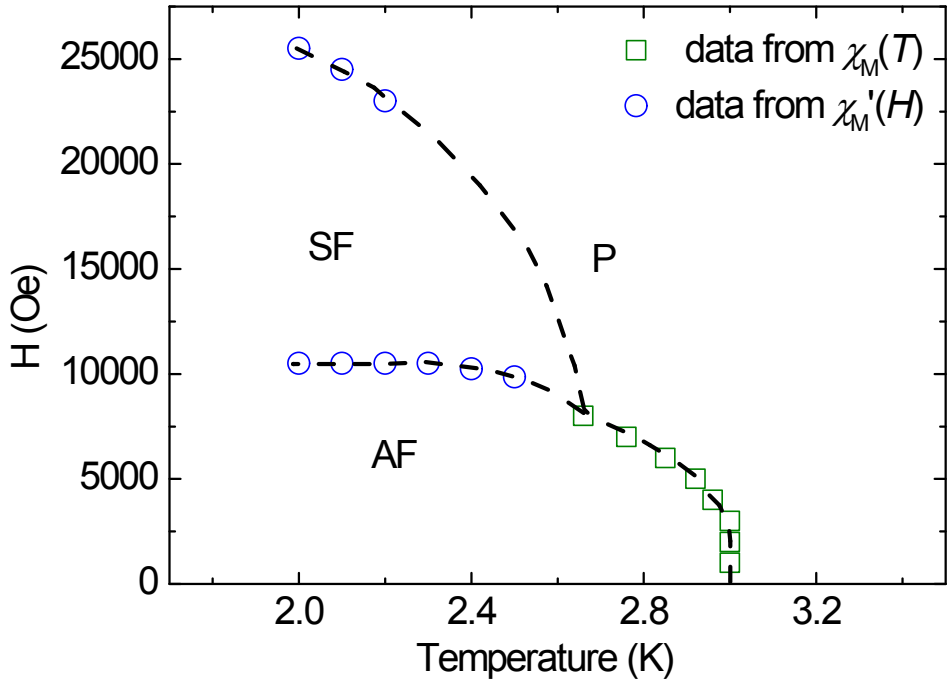

Fig. S13. Magnetic phase (T, H) diagram for **2·Mn**, the data obtained from location of the maximum of $\chi_M(T)$ data (open green square) and location of the maximum of $\chi_M'(H)$ (open blue circle); the solid line is a guide.

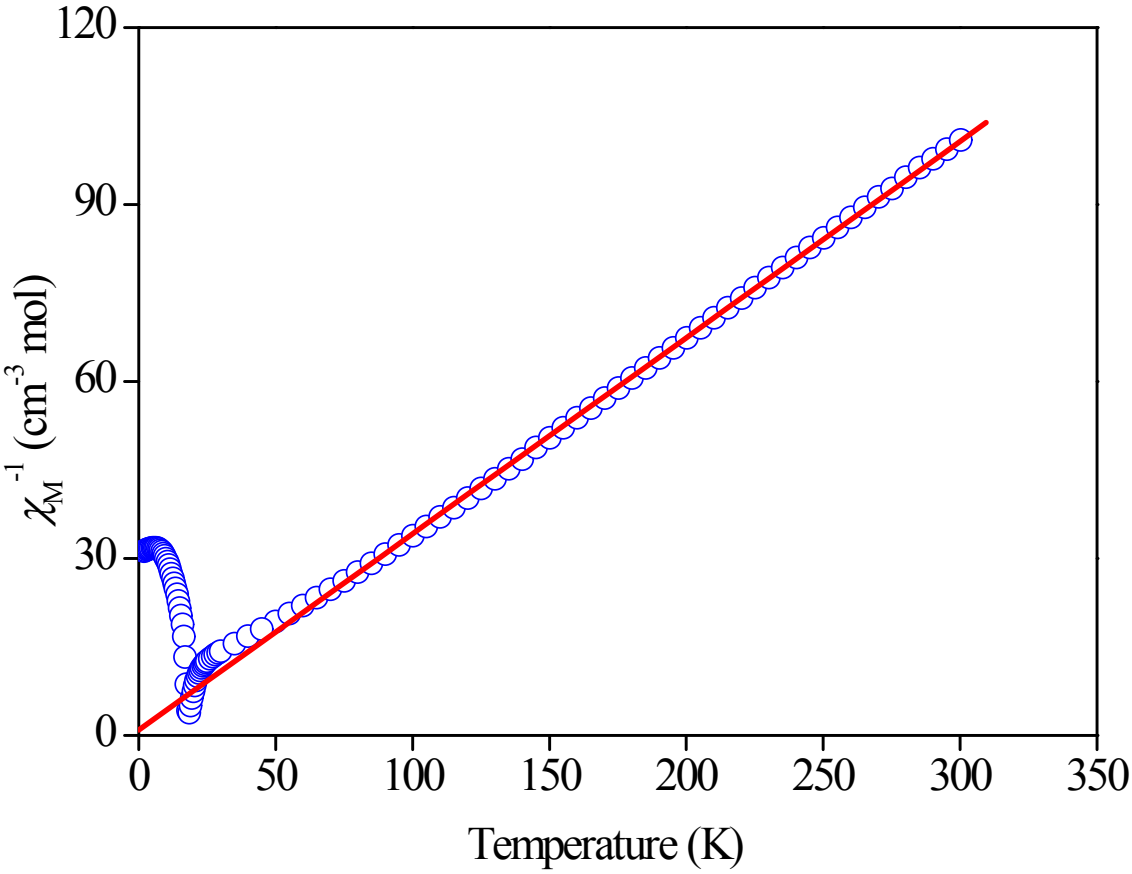

Fig. S14. Plot of χ_M^{-1} (○) vs. *T* of compound **3·Co**. The solid line represents the best fit χ_M^{-1} above 50 K with a Curie–Weiss law.

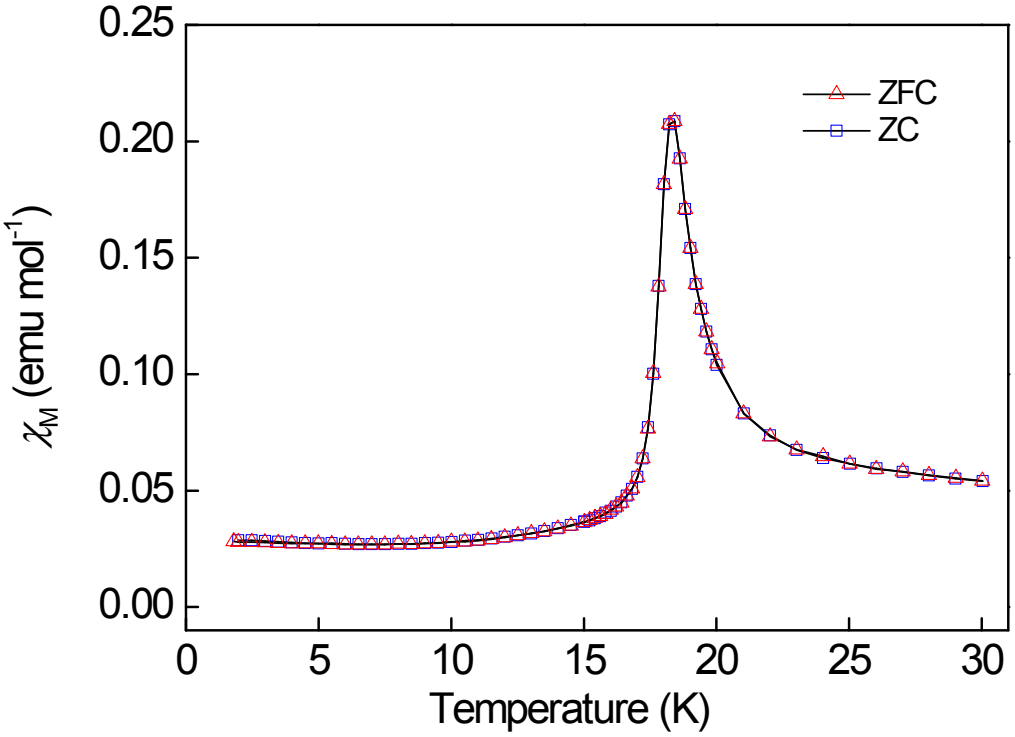

Fig. S15. ZFC/FC magnetizations of compound **3·Co** at 100 Oe.

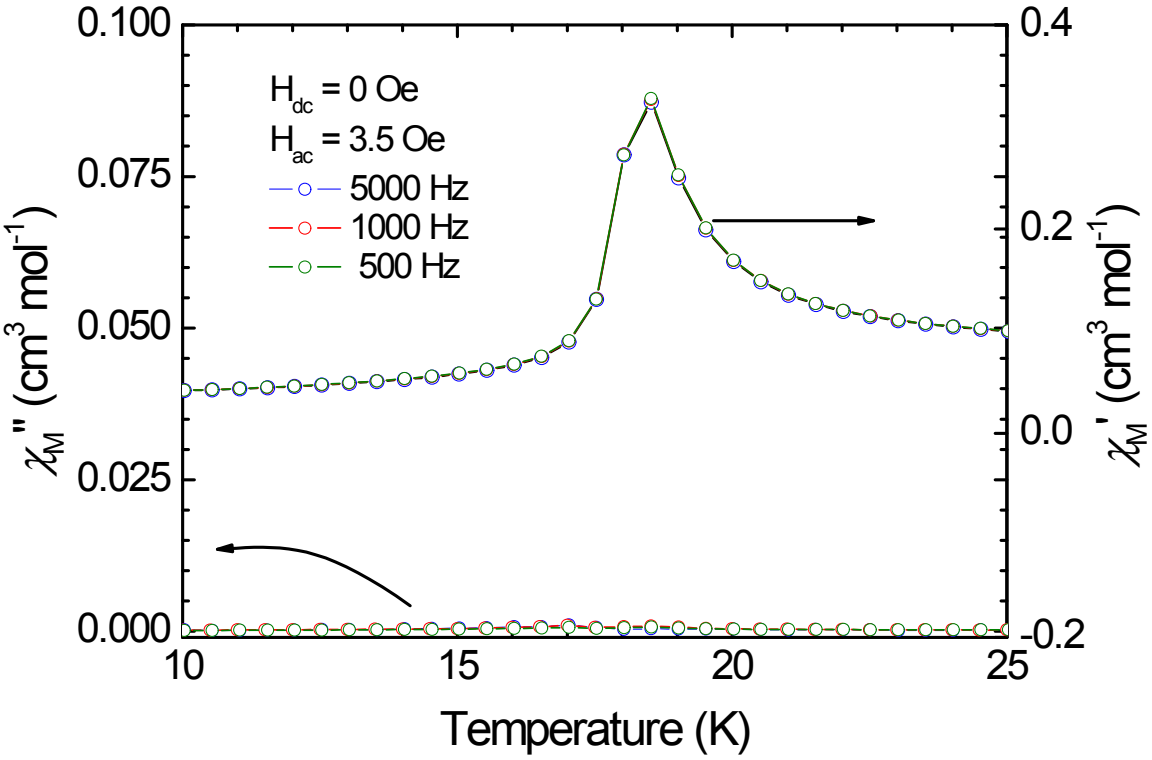

Fig. S16. In phase (χ') and out-off phase (χ'') ac magnetic susceptibilities in a zero applied dc field and in an ac field of 3.5 G at the indicated frequencies for **3·Co**.

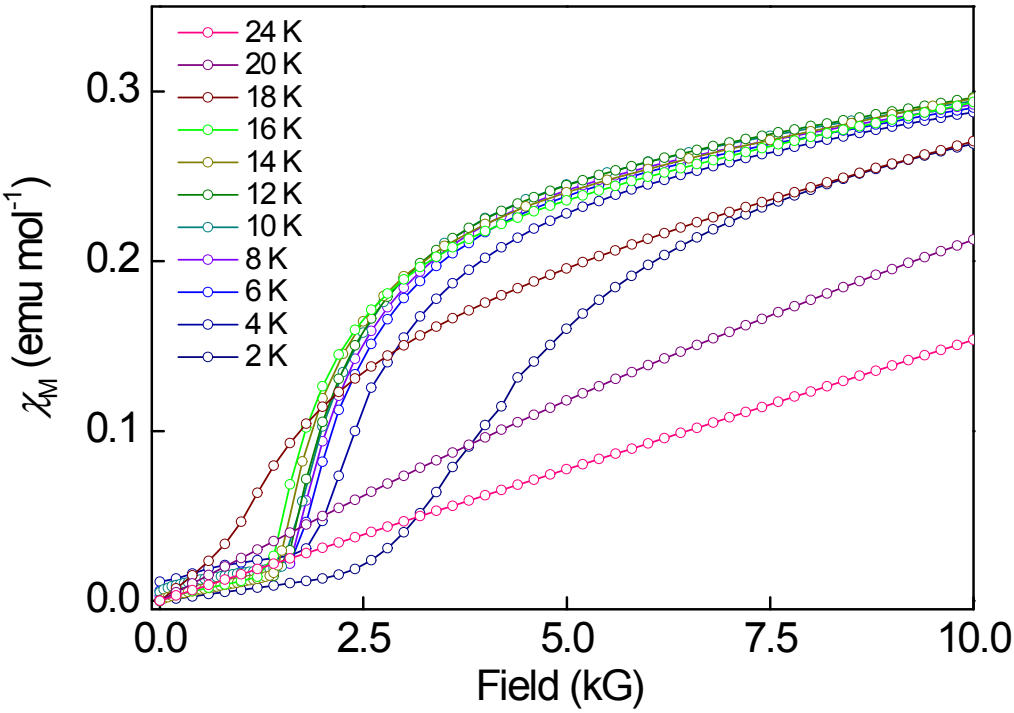

Fig. S17. Field dependence of magnetizations for compound **3·Co** measured at the indicated temperatures.

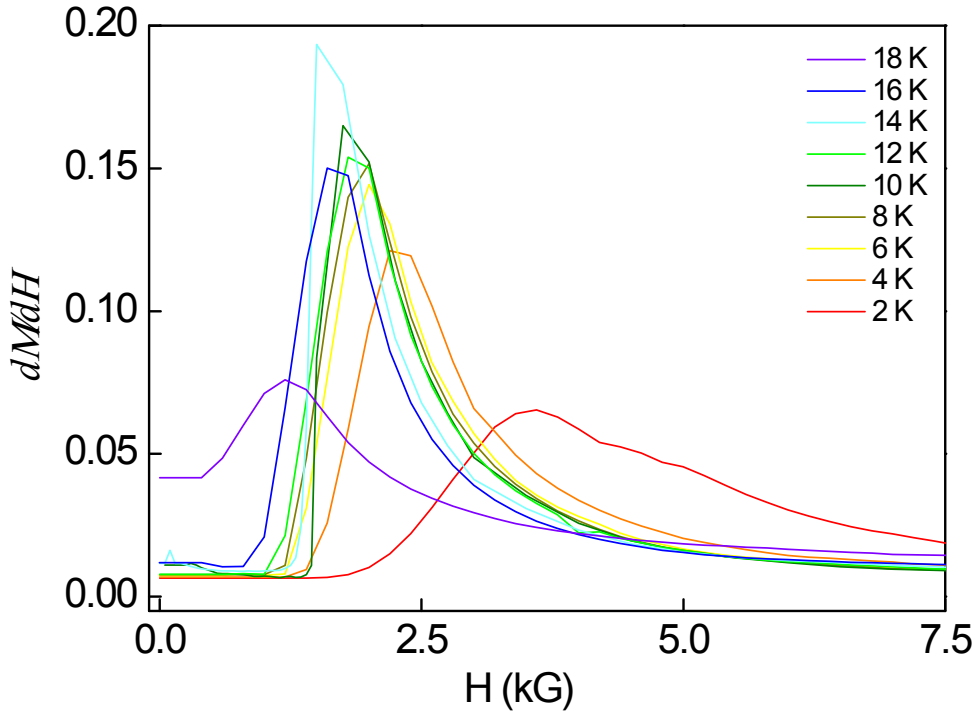

Fig. S18. d*M*/d*H* vs. *H* plots for the virgin magnetization of compound **3·Co**.

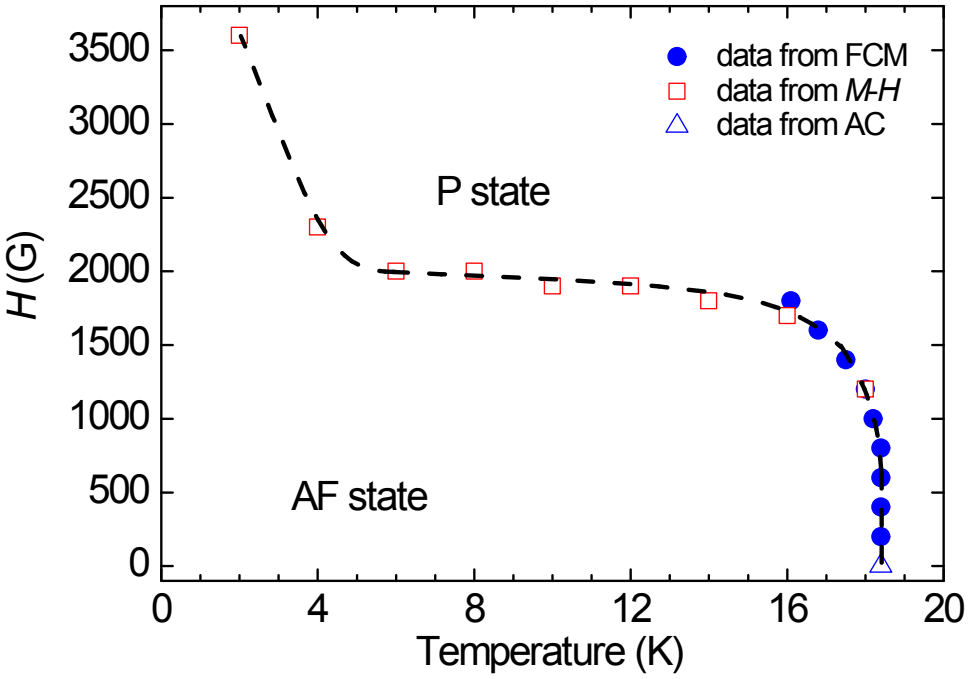

Fig. S19. Magnetic phase (*T, H*) diagram for **3·Co**, the data from location of the maximum of susceptibility from χ_M vs *T* data (filled blue circle), location of the maximum of susceptibility from d*M*/d*H* vs *H* data (open blue square) and ac data (open blue triangle); the solid line is a guide.